Chinese Chemical Letters 36 (2025) 109910

Contents lists available at ScienceDirect

Chinese Chemical Letters

journal homepage: www.elsevier.com/locate/cclet

Three-in-one erlotinib-modified NIR photosensitizer for fluorescence imaging and synergistic chemo-photodynamic therapy

Du Liu, Yuyan Li, Hankun Zhang, Benhua Wang*, Chaoyi Yao*, Minhuan Lan, Zhanhong Yang, Xiangzhi Song*

College of Chemistry & Chemical Engineering, Central South University, Changsha 410083, China

ARTICLE INFO

Article history:
Received 29 February 2024
Revised 16 April 2024
Accepted 18 April 2024
Available online 21 April 2024

Keywords:
Photosensitizer
Benzo[*a*]phenoselenazinium
Fluorescence imaging
Photodynamic therapy
Chemotherapy

ABSTRACT

Photodynamic therapy (PDT) presents a promising avenue in cancer treatment. Erlotinib, an FDA-approved anticancer drug targeting epidermal growth factor receptor (EGFR), has shown effectiveness in normalizing tumor vasculature across various tumors, thereby promoting tumor oxygenation and facilitating PDT. In this work, erlotinib was conjugated with a near-infrared (NIR) photosensitizer, benzo[*a*]phenoselenazinium, yielding three EGFR-targeted PDT agents (**NBSe-nC-Er**). These newly synthesized photosensitizers demonstrate specificity in binding to EGFR, thereby enhancing their accumulation in cancer cells and tumors, and consequently improving the efficiency of both PDT and chemotherapy. Additionally, the NIR fluorescence emitted by the photosensitizer allows for imaging-guided therapy, offering a non-invasive means of monitoring treatment progress. The distinctive properties of the three-in-one photosensitizer render it an ideal candidate for precise tumor treatment, overcoming the limitations of conventional therapies.

Epidermal growth factor receptor (EGFR), a transmembrane glycoprotein in the tyrosine kinase family located on the surface of the cell membrane, is highly expressed in cancers like non-small cell lung cancer and pancreatic cancer [1–3]. Therefore, EGFR has emerged as an important target in cancer therapy, and various EGFR treatment strategies, including chemotherapy and monoclonal antibody immunotherapy, have been developed clinically [4,5]. Erlotinib (Er), a Food and Drug Administration (FDA)-approved anticancer drug targeting the adenosine triphosphate (ATP) binding domain of EGFR, has demonstrated promising anticancer efficacy in various types of cancers [6,7]. However, drug resistance occurs inevitably after long-term use of EGFR-targeted therapies, significantly limiting their clinical efficacy [8–11]. Therefore, further development of EGFR-targeted therapy relies on adopting other cancer treatments to combat tumors in a coordinated and multifaceted manner.

Photodynamic therapy (PDT), utilizing a combination of light, photosensitizer (PS), and oxygen, stands out as a promising treatment due to non-invasiveness and minimal drug resistance [12–19]. Despite extensive research into PDT, its therapeutic efficacy is hindered by the selective accumulation of PS and the reduced oxygen level within the tumors [20–24]. EGFR can be used as a good target to enhance the effectiveness of PDT as it is amplified and overexpressed in various tumors. On the one hand, EGFR targeting increases the selectivity of PS towards tumor cells; on the other hand, EGFR inhibitors enhance apoptosis and inhibit the proliferation of tumors treated with PDT [25–28]. More importantly, EGFR-targeted therapies can effectively normalize tumor vasculature, promoting tumor oxygenation and thus enhancing PDT [29,30].

Currently, two main strategies are used to combine PDT and EGFR-targeted therapy. One is by employing nanoparticles modified with target moieties as carriers of PSs, and the other is by conjugating the PSs to drugs through covalent bonding [31–35]. The complex procedure of controlling the size, stability, drug loading, and releasing ability of nanoparticles makes them less precise than PSs possessing inherent targeting properties, while covalently binding drugs with PSs simplifies this issue [36,37]. Some researchers have covalently attached Er to conventional PSs such as porphyrin, chlorin, and phthalocyanine to improve cancer treatments [32,34,35]. However, these PSs have relatively short excitation and emission wavelengths, limited tissue penetration ability, and tend to form aggregates in aqueous media.

Benzo[*a*]pheno-thiazinium dye (EtNBS, Scheme 1), has garnered significant attention as a potent anticancer agent, undergoing extensive study both within our research group and by other re-

* Corresponding authors.
E-mail addresses: benhuawang@csu.edu.cn (B. Wang), chaoyiyao@csu.edu.cn (C. Yao), xzsong@csu.edu.cn (X. Song).

https://doi.org/10.1016/j.cclet.2024.109910
1001-8417/

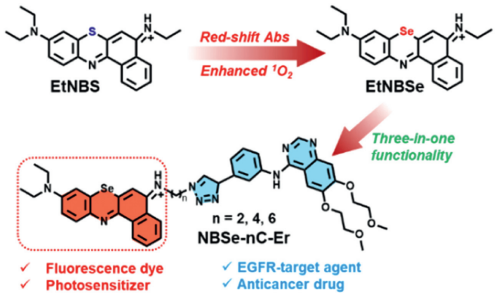

Scheme 1. Rational design of the three-in-one PS **NBSe-nC-Er** for NIR fluorescence imaging and synergistic chemo-photodynamic therapy.

searchers [38–42]. Benzo[*a*]phenoselenazinium (EtNBSe, Scheme 1) is an analog of EtNBS, exhibiting superior singlet oxygen ($^1O_2$) yield and possessing intense absorption and emission properties in the near-infrared (NIR) region [43,44]. This characteristic allows for enhanced tissue penetrate on in living organisms, enabling deeper delivery and potential therapeutic applications. Despite these advantageous features, the biological applications of EtNBSe have been relatively underexplored.

Herein, we have covalently conjugated EtNBSe dye with Er to develop three NIR PSs, designated as **NBSe-nC-Er** ($n = 2$, 4, 6), with improved anticancer capabilities (Scheme 1). It was hypothesized that the targeting ability of Er would facilitate the delivery of PSs to EGFR-overexpressed cancer cells, thereby improving the selectivity of PDT. Additionally, the synergistic effect of Er's chemotherapy and EtNBSe's PDT was expected to enhance the overall treatment efficacy of the PSs. Furthermore, the NIR fluorescence exhibited by **NBSe-nC-Er** allows for imaging-guided therapy, thereby adding a multifunctional aspect to enable precise cancer treatment.

To evaluate the potential influence of the linker length between EtNBSe dye and Er on their binding mode towards EGFR, three PSs with alkyl chains of different lengths, denoted as **NBSe-nC-Er** ($n = 2$, 4, 6), were designed. Synthesis of PS **NBSe-nC-Er** is shown in Scheme S1 (Supporting information). Firstly, α-naphthylamine was substituted with 1-bromo-2-azidoethane, 1-bromo-4-azidbutane, and 1-bromo-6-azido-hexane to afford the corresponding azidated naphthylamines of different chain lengths. Treatment of the corresponding compounds with bis-(3-*N*,*N*-diethylamino-6-nitrosophenyl)diselenide **2** gave **NBSe-nC-N_3**, which were then subjected to click reaction with Er to obtain the three PSs **NBSe-nC-Er**. The chemical structures were characterized by ^{1}H nuclear magnetic resonance (NMR), ^{13}C NMR, and high resolution mass spectrum (HRMS).

All PSs exhibited intense absorptions around 660 nm and NIR fluorescence with $\lambda_{max} = 710$ nm in water (Fig. 1a). Therefore, these PSs could be activated by the light within the "therapeutic window" (650–900 nm), enabling light penetration into deeper biological tissues. Besides, **NBSe-nC-Er** showed good water solubility of about 0.2 g/L and the lipo-solubility, characterized by the octanol/water partition coefficient (K_{ow}), of around 4.0 (Fig. S1 and Table S1 in Supporting information). We further evaluated the photostability of the three PSs. As illustrated in Fig. S2 (Supporting information), **NBSe-4C-Er** and **NBSe-6C-Er** exhibited superior resistance to photodegradation compared to **NBSe-2C-Er**. Consequently, the EtNBSe-based dyes demonstrated favorable characteristics including good water-solubility, lipo-solubility, and photostability, rendering them suitable for biological applications.

The $^1O_2$ generation capacity of PSs is one of the most straightforward parameters to assess their PDT efficacy. Therefore, we evaluated the $^1O_2$ generation capacity of **NBSe-nC-Er** using 1,3-diphenylisobenzofuran (DPBF) as a $^1O_2$ probe in air-saturated methanol under 650 nm Xe lamp irradiation. The absorbance of

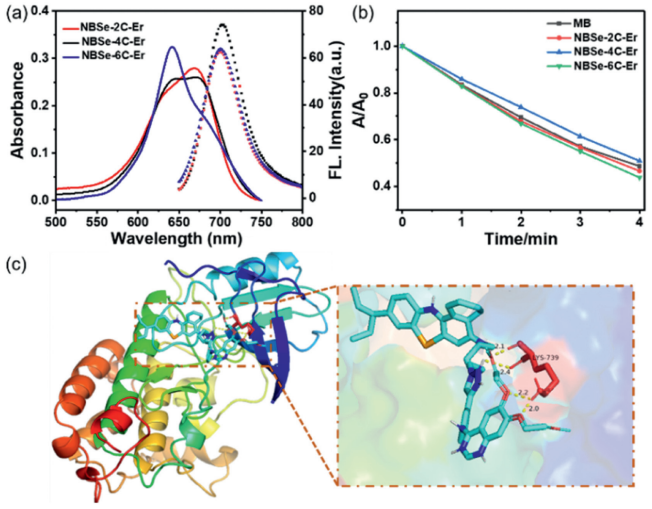

Fig. 1. (a) UV–vis absorption (solid lines) and fluorescence emission (dashed lines) spectra of **NBSe-nC-Er** in water. (b) Decline of DPBF absorption at 411 nm in the presence of various PSs. (c) The molecular docking results of **NBSe-6C-Er** towards EGFR.

DPBF at 411 nm remained unchanged in the absence of PS (Fig. S3 in Supporting information). However, upon addition of **NBSe-nC-Er** solution followed by 650 nm irradiation, the 411 nm absorption of DPBF decreased rapidly, indicating the oxidation of DPBF by the generated $^1O_2$ (Fig. 1b and Fig. S4 in Supporting information). The calculated singlet oxygen yields (Φ_Δ) of **NBSe-2C-Er**, **NBSe-4C-Er**, and **NBSe-6C-Er** were as high as 75.9%, 73.3%, and 66.7%, respectively. The similar Φ_Δ values of the three PSs suggested that the introduction of Er and the length of the linker had little effect on the photophysical properties of EtNBSe.

To assess whether the linker in **NBSe-nC-Er** affects its binding mode towards EGFR, molecular docking calculations on **NBSe-nC-Er** and EGFR kinase domain were performed using AutoduckTools-1.5.6 and Pymol. The binding patterns of the three **NBSe-nC-Er** conjugates to EGFR were similar: the EtNBSe portion occupied the ATP-binding cleft through hydrophobic interactions. The only distinction was observed in the formation of hydrogen bonds between the Er moiety and different residues in the three conjugates (Fig. 1c, Figs. S5 and S6 in Supporting information). Additionally, the binding energies of **NBSe-2C-Er**, **NBSe-4C-Er**, and **NBSe-6C-Er** with EGFR were determined to be −7.0, −5.0, and −6.2 kcal/mol, respectively (Table S2 in Supporting information). These findings suggest that the length of the linkage chain can influence the binding mode and potency of the PS with EGFR.

Due to **NBSe-6C-Er**'s favorable photophysical properties and good EGFR targeting ability, it was selected for subsequent biological analysis. For comparison, PS **NBSe-6C** without the Er moiety was prepared using the same method as a reference (Fig. S7 in Supporting information). The tumor selectivity of PSs **NBSe-6C-Er** and **NBSe-6C** was evaluated by assessing their targeted cellular uptake in A549, MCF-7, and L929 cells with varying EGFR expression levels (A549 > MCF-7 > L929). After incubating the cells with **NBSe-6C-Er** and **NBSe-6C** separately for 30 min, confocal fluorescence imaging was conducted. The fluorescence intensity of **NBSe-6C-Er** in cells was positively correlated with the EGFR expression levels, as displayed in Fig. 2. However, cells treated with **NBSe-6C** displayed weak red fluorescence across all three cell lines. Importantly, the fluorescence in A549 cells pre-treated with Er to mask the binding sites of EFGR and subsequently incubated with **NBSe-6C-Er** was notably suppressed. These results confirm that **NBSe-6C-Er** binds to cancer cells through specific binding with EGFR, and the conjugation of Er enhances its cellular uptake.

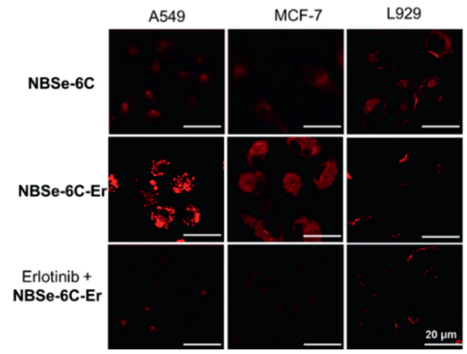

Fig. 2. Fluorescence images of A549, MCF-7, and L929 cells with different treatments. $\lambda_{ex} = 640$ nm, $\lambda_{em} = 650–750$ nm. Scale bar: 20 μm.

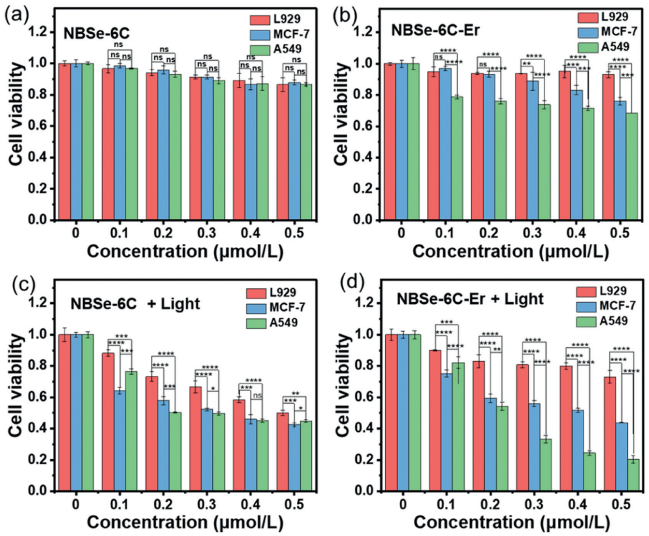

Fig. 3. Cell viability of cells incubated with different concentrations of **NBSe-6C** (a, c) and **NBSe-6C-Er** (b, d) in the absence and presence of light irradiation (640–660 nm, 20 mW/cm^2). Data are expressed as means ± SD ($n = 6$), n.s., no significance. $^*P < 0.05$, $^{**}P < 0.01$, $^{***}P < 0.001$, $^{****}P < 0.0001$.

The effectiveness of PSs **NBSe-6C-Er** and **NBSe-6C** were then determined using the standard methyl thiazolyl tetrazolium (MTT) assay under light emitting diode (LED) light (640–660 nm, 20 mW/cm^2). **NBSe-6C** exhibited minimal dark toxicity, with a killing degree of approximately 10% for all three cell lines (Fig. 3a). The independent chemotherapeutic effect of Er was evaluated, showing a gradual increase in cellular mortality rates with increasing EGFR expression levels (Fig. S8 in Supporting information). The conjugation of Er to EtNBSe in **NBSe-6C-Er** exhibited chemotherapeutic effects similar to those of Er alone (Fig. 3b). Under light irradiation, the mortality rates of cells incubated with PS **NBSe-6C** (0.5 μmol/L) for 24 h were approximately 50% for all three cell lines (Fig. 3c). Treatment with PS **NBSe-6C-Er** (0.5 μmol/L) resulted in killing degrees of 80%, 50%, and 30% for A549, MCF-7, and L929 cells, respectively (Fig. 3d and Table S3 in Supporting information). However, the potency of PS **NBSe-6C-Er** under light irradiation decreased when pre-treated with Er for 30 min, followed by incubation with **NBSe-6C-Er** for another 20 min. In this case, a cell killing rate of only 57% and 40% was achieved for A549 and MCF-7 cells, respectively (Fig. S9 in Supporting information). These results demonstrate that **NBSe-6C-Er** can selectively and effectively kill cancer cells due to the targeting and chemotherapeutic effects of Er, compared to its counterpart **NBSe-6C**, which indiscriminately killed all cells.

To assess the subcellular distribution of **NBSe-6C-Er**, we co-stained A549 cells with commercial fluorescent dyes. As shown in Fig. S10 (Supporting information), the fluorescence image stained by **NBSe-6C-Er** matched well with that of Lyso-tracker Green, indicating that **NBSe-6C-Er** can target lysosomes. The photodynamic therapeutic effects of PSs were further assessed using live/dead cell co-staining assays. Propidium iodide (PI) stains dead cells, emitting red fluorescence, whereas live cells are stained by calcein-AM, emitting green fluorescence. As depicted in Fig. S11 (Supporting information), A549 cells treated with Er primarily displayed green fluorescence, indicating that Er inhibited the proliferation of cancer cells without inducing cell death directly. Cells treated with PSs **NBSe-6C** and **NBSe-6C-Er** under dark conditions also displayed intense green fluorescence, suggesting minimal dark toxicity. However, upon light irradiation, **NBSe-6C**-treated cells displayed both red and green fluorescence, whereas only strong red fluorescence was observed from **NBSe-6C-Er**-treated cells. This implies that the synergistic effect of chemotherapy and PDT is more effective than individual treatments. Cell migration assays further underscored **NBSe-6C-Er**'s ability to impede wound healing and cell migration on A549 and MCF-7 cells, demonstrating its potent anti-cancer effect, particularly in EGFR-overexpressed cells (Fig. S12 in Supporting information). These findings emphasize the enhanced therapeutic potential of **NBSe-6C-Er** through the synergistic chemotherapy and PDT.

Building upon the promising *in vitro* results, the photodynamic therapy effect of PS **NBSe-6C-Er** was evaluated *in vivo* using A549 tumor-bearing mice as a model. All related animal experiments were performed according to guidelines approved by the Ethics Committee of Hunan Normal University. After administering PSs **NBSe-6C** and **NBSe-6C-Er** *via* the tail vein, fluorescence imaging experiments were conducted on mice at different time points. As illustrated in Fig. 4a, fluorescent signals from the tumor were detectable 1 h post-injection of **NBSe-6C** or **NBSe-6C-Er** and intensified over time, reaching a maximum at approximately 2 h. Noteworthy, the tumors treated with **NBSe-6C-Er** exhibited red fluorescence 1.25-fold stronger than those treated with **NBSe-6C** (Fig. 4b). **NBSe-6C-Er**-treated tumors maintained strong red fluorescence even at 4 h post-injection, while fluorescence from **NBSe-6C**-treated tumors diminished. These results underscore the effective tumor targeting and enhanced accumulation of **NBSe-6C-Er** at the tumor site.

Finally, the antitumor effect of PS **NBSe-6C-Er** was investigated on A549 tumor-bearing mice. Following anesthesia, mice in each group were injected with PBS, Er or PSs *via* the tail vein and irradiated with LED lamp for 20 min. The tumor size and weight of the mice were measured each day for 14 days. As depicted in Fig. 4c, the tumors of mice injected with PBS exhibited rapid growth, whereas mice injected with Er or **NBSe-6C-Er** without light irradiation showed slight inhibition in tumor growth, indicating the chemotherapy effects of Er. However, **NBSe-6C-Er** treatment significantly suppressed tumors growth compared to **NBSe-6C** treatment under light irradiation (Fig. 4d). Furthermore, the body weight of all mice varied slightly throughout the different treatments (Fig. 4e). The apoptosis of tumor cells and any damage to organs (heart, liver, spleen, lung, and kidneys) caused by **NBSe-6C-Er** after PDT was investigated using hematoxylin & eosin (H&E) staining. As evidenced in Fig. S13 (Supporting information), destructive cell necrosis was observed in the tumor tissue, while no significant histologic changes were observed in the major organs of **NBSe-6C-Er**-treated mice.

Er has demonstrated efficacy in normalizing tumor vasculature in various tumors by inhibiting EGFR and down-regulating vascular endothelial growth factor (VEGF) [29,30]. Subsequently, the content of VEGF in tumor sections after different treatments was studied by immunohistochemistry. Fig. 4f demonstrated a reduction in

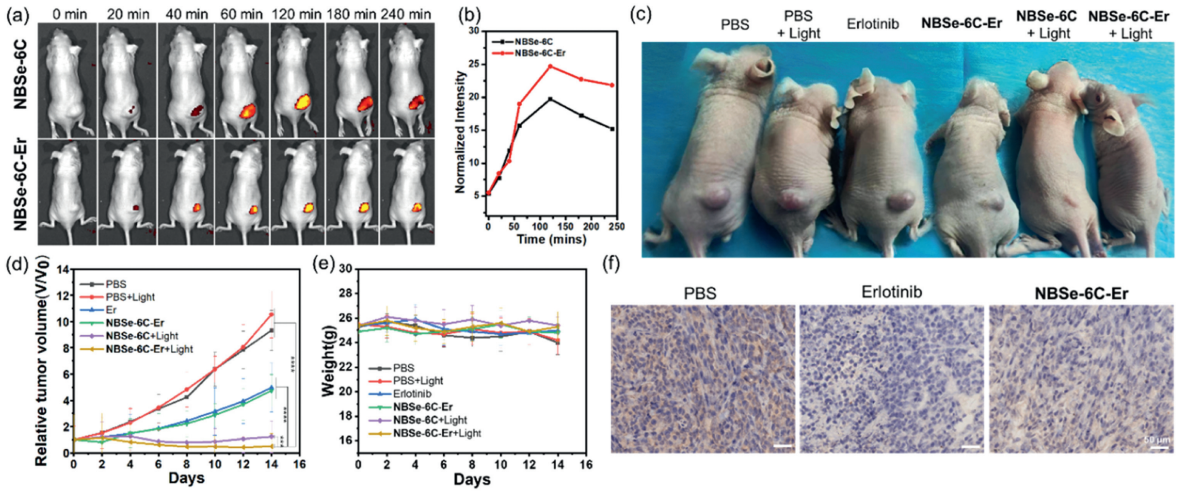

Fig. 4. (a) NIR Fluorescence images of tumor-bearing mice treated with PSs **NBSe-6C** and **NBSe-6C-Er** (100.0 μL, 10.0 μmol/L) at different time points. $\lambda_{ex} = 640$ nm, $\lambda_{em} = 680–720$ nm. (b) Quantitative image analysis of average fluorescence intensity of tumors. (c) Photographs depicting mice subjected to different treatments. (d) Plots of the relative tumor volume of mice over time following different treatments. (e) Plots of the body weights of mice over time after different treatments. (f) Immunohistochemical staining of VEGF in tumor tissues obtained from the mice receiving different treatments. Scale bar: 50 μm. Data are expressed as means ± SD ($n = 3$), $^{***}P < 0.001$, $^{****}P < 0.0001$.

VEGF content (brown-yellow region) in both the Er and **NBSe-6C-Er** groups, suggesting that Er can suppress VEGF expression by targeting EGFR and alleviate hypoxia by improving intratumor blood perfusion. These results prove the high biocompatibility and efficacy of **NBSe-6C-Er** in anticancer therapy.

In summary, we have designed and synthesized three NIR PSs, **NBSe-nC-Er** ($n = 2$, 4, 6), through the conjugation of EtNBSe dye with Er, serving as both the tumor-targeting ligand and chemotherapy agent, *via* alkyl chains of varying lengths. The enhanced targeting ability of **NBSe-6C-Er** led to improved uptake by cancer cells and reduced side effects on normal cells. Furthermore, the chemotherapy effect of Er synergistically enhanced the PDT effect, resulting in a combined chemotherapy and photodynamic therapy approach. The *in vitro* and *in vivo* experiments underscored the potential of **NBSe-6C-Er** as a promising anticancer agent for precise cancer treatments. The present research aims to contribute insights into optimizing the design and performance of PSs to enhance the efficacy of combined EGFR-targeted chemotherapy and photodynamic therapy.

Declaration of competing interest

The authors declare that they have no known competing financial interests or personal relationships that could have appeared to influence the work reported in this paper.

CRediT authorship contribution statement

Du Liu: Writing – original draft, Investigation, Conceptualization. **Yuyan Li:** Formal analysis, Data curation. **Hankun Zhang:** Methodology. **Benhua Wang:** Writing – review & editing, Supervision, Funding acquisition. **Chaoyi Yao:** Writing – review & editing, Conceptualization. **Minhuan Lan:** Visualization. **Zhanhong Yang:** Supervision. **Xiangzhi Song:** Writing – review & editing, Supervision.

Acknowledgments

This work was supported by the National Natural Science Foundation of China (Nos. 22278447 and 22178395), State Key Laboratory of Fine Chemicals (No. KF2109) and State Key Laboratory of Chemo/Biosensing and Chemometrics (No. 20230768).

Supplementary materials

Supplementary material associated with this article can be found, in the online version, at doi:10.1016/j.cclet.2024.109910.

References

[1] J. Chen, F. Zeng, S.J. Forrester, et al., Physiol. Rev. 96 (2016) 1025–1069.
[2] T. Yamaoka, M. Ohba, T. Ohmori, Int. J. Mol. Sci. 18 (2017) 2420.
[3] M.K. Mayekar, T.G. Bivona, Clin. Pharmacol. Ther. 102 (2017) 757–764.
[4] Q. He, M. Qu, H. Bao, et al., Cytokine Growth Factor Rev. 70 (2023) 41–53.
[5] Q. Guo, L. Liu, Z. Chen, et al., Front. Oncol. 12 (2022) 945102.
[6] K.H. Dragnev, W.J. Petty, S. Shah, et al., J. Clin. Oncol. 23 (2005) 8757–8764.
[7] M.H. Cohen, J.R. Johnson, Y.F. Chen, et al., Oncologist 10 (2005) 461–466.
[8] M. Bersanelli, R. Minari, P. Bordi, et al., J. Thorac. Oncol. 11 (2016) e121–e123.
[9] A. Ramos, S. Sadeghi, H. Tabatabaeian, Int. J. Mol. Sci. 22 (2021) 9451.
[10] H.A. Yu, S.K. Tian, A.E. Drilon, et al., JAMA Oncol. 1 (2015) 982–984.
[11] A.N. Hata, M.J. Niederst, H.L. Archibald, et al., Nat. Med. 22 (2016) 262–269.
[12] X. Zhao, J. Liu, J. Fan, et al., Chem. Soc. Rev. 50 (2021) 4185–4219.
[13] G. Feng, G.Q. Zhang, D. Ding, Chem. Soc. Rev. 49 (2020) 8179–8234.
[14] T.C. Pham, V.N. Nguyen, Y. Choi, et al., Chem. Rev. 121 (2021) 13454–13619.
[15] T. Hu, C. Shen, X. Wang, et al., Chin. Chem. Lett. 35 (2024) 109562.
[16] W. Liu, Y. Hou, W. Liu, et al., Chin. Chem. Lett. 35 (2024) 109631.
[17] D. Zhang, K.X. Teng, L. Zhao, et al., Adv. Mater. 35 (2023) 2209789.
[18] S. Su, X. Li, Q. An, et al., Chem. Commun. 60 (2024) 3910–3913.
[19] S.Y. Wang, Y.H. Pan, Y.C. Qu, et al., Smart Mol. 2 (2024) e20230024.
[20] L. Huang, S. Zhao, J. Wu, et al., Coord. Chem. Rev. 438 (2021) 213888.
[21] J.H. Correia, J.A. Rodrigues, S. Pimenta, et al., Pharmaceutics 13 (2021) 1332.
[22] Q. Zhao, G. Qing, J. Yu, et al., Chin. Chem. Lett. 35 (2024) 108535.
[23] W. Su, X. Luo, P. Li, et al., Chin. Chem. Lett. 35 (2024) 109522.
[24] K.X. Teng, D. Zhang, B.K. Liu, et al., Angew. Chem. Int. Ed. 63 (2024) e202318783.
[25] P.V. Nguyen, K. Hervé-Aubert, I. Chourpa, et al., Int. J. Pharm. 609 (2021) 121134.
[26] S.M. Gallagher-Colombo, J. Miller, K.A. Cengel, et al., Cancer Res. 75 (2015) 3118–3126.
[27] L. Ulfo, P.E. Costantini, M. Di Giosia, et al., Pharmaceutics 14 (2022) 241–285.
[28] L. Yan, J. Miller, M. Yuan, et al., Biomacromolecules 18 (2017) 1836–1844.
[29] Q. Chen, L. Xu, J. Chen, et al., Biomaterials 148 (2017) 69–80.
[30] Y. Liu, X. Ma, Y. Zhu, et al., Chem. Eng. J. 437 (2022) 135305.
[31] M.R. Younis, G. He, J. Qu, et al., Adv. Sci. 8 (2021) 2102587.
[32] F.L. Zhang, Q. Huang, K. Zheng, et al., Chem. Commun. 49 (2013) 9570–9572.
[33] E.Y. Gül, E.A. Karataş, H.A. Doğan, et al., ChemMedChem 18 (2023) e202200439.
[34] B.G. Ongarora, K.R. Fontenot, X. Hu, et al., J. Med. Chem. 55 (2012) 3725–3738.
[35] R.R. Cheruku, J. Cacaccio, F.A. Durrani, et al., J. Med. Chem. 62 (2019) 2598–2617.
[36] J. Shi, P.W. Kantoff, R. Wooster, et al., Nat. Rev. Cancer 17 (2017) 20–37.

[37] M. Xu, Y. Qi, G. Liu, et al., ACS Nano 17 (2023) 20825–20849.
[38] M. Li, T. Xiong, J. Du, et al., J. Am. Chem. Soc. 141 (2019) 2695–2702.
[39] C. Shi, X. Zhou, Q. Zhao, et al., CCS Chem. 4 (2022) 2662–2673.
[40] X. Yue, B. Wang, M. Lan, et al., Chem. Commun. 59 (2023) 4676–4679.
[41] X. Yue, T. Guo, H. Zhang, et al., Chem. Commun. 59 (2023) 7060–7063.
[42] Y. Li, Z. Gao, X. Yue, et al., Chin. Chem. Lett. 35 (2024) 109133.
[43] K.H. Gebremedhin, M. Li, F. Gao, et al., Dyes Pigm. 170 (2019) 107617.
[44] J.W. Foley, X. Song, T.N. Demidova, et al., J. Med. Chem. 49 (2006) 5291–5299.